Generation of spin-triplet Cooper pairs via a canted antiferromagnet

Simran Chourasia,[1,*] Lina Johnsen Kamra,[2,1] Irina V. Bobkova,[3,4] and Akashdeep Kamra[1]
[1]*Condensed Matter Physics Center (IFIMAC) and Departamento de Física Teórica de la Materia Condensada, Universidad Autónoma de Madrid, E-28049 Madrid, Spain*
[2]*Center for Quantum Spintronics, Department of Physics, Norwegian University of Science and Technology, NO-7491 Trondheim, Norway*
[3]*Moscow Institute of Physics and Technology, Dolgoprudny, 141700 Moscow, Russia*
[4]*Department of Physics, National Research University Higher School of Economics, Moscow 101000, Russia*

(Received 31 March 2023; accepted 9 August 2023; published 22 August 2023)

Spinful triplet Cooper pairs can be generated from their singlet counterparts available in a conventional superconductor (S) using two or more noncollinear magnetic moments, typically contributed by different magnets in a multilayered heterostructure. Here, we theoretically demonstrate that a S interfaced with a canted antiferromagnet (AFM) harbors spinful triplet Cooper pairs capitalizing on the intrinsic noncollinearity between the two AFM sublattice magnetizations. As the AFM canting can be controlled by an applied field, our paper proposes a simple bilayer structure that admits controllable generation of spin-triplet Cooper pairs. Employing the Bogoliubov–de Gennes framework, we delineate the spatial dependence of the spin-triplet correlations. We further evaluate the superconducting critical temperature as a function of the AFM canting, which provides one experimental observable associated with the emergence of these triplet correlations.

DOI: 10.1103/PhysRevB.108.064515

I. INTRODUCTION

The dissipationless flow of charge in superconductors is partly responsible for their central role in various emerging quantum technologies [1,2]. The widely available conventional superconductors, such as Al and Nb, are made of spin-singlet Cooper pairs, which harbor no net spin [3]. A superconductor hosting spin-triplet Cooper pairs can support dissipationless spin currents [4–8], deemed valuable for switching magnetic memories [9–13], as well as exotic excitations, such as Majorana bound states [14,15]. Such an unconventional superconductor can be engineered from its conventional counterpart employing heterostructures incorporating magnetic multilayers [5–8,16]. The basic requirement for achieving spinful triplets from spin singlets is exposing the latter to two or more noncollinear spin-splitting fields. A wide variety of multilayered hybrids comprising conventional superconductors (S) and ferromagnets (FMs) has been employed to achieve the desired spinful triplets [17–33], coming a long way from the initial critical temperature studies [34,35].

Since a Néel-ordered antiferromagnet (AFM) bears no net spin or magnetic moment, for some time it was considered inert at causing spin splitting in an adjacent S. Indeed, early experiments found a metallic AFM to behave just like a normal metal when considering its effect on an adjacent S [36]. More recent experiments, on the other hand, found the AFM to substantially affect the adjacent S with intriguing dependencies [37–42]. From the theory perspective, Josephson junctions [43,44] and interfaces [45,46] involving itinerant AFMs were shown to exhibit nontrivial properties due to quasiparticle reflections. Moreover, a recent work demonstrated that an uncompensated interface of an insulating AFM with an adjacent S induces a strong spin-splitting as well as spin-flip scattering thereby strongly influencing the S [47]. Subsequent work found even the fully compensated interface between the AFM and S to be spin active [48]. This has been understood to be due to the AFM inducing Néel triplets whose pairing amplitude has an alternating sign in space similar to the AFM spin [49]. Altogether, the potential usefulness of AFMs [50] in engineering unique superconducting effects and devices, such as a filter [51], is starting to be understood.

Pekar and Rashba [52] recognized long ago that even though the net spin vanishes in an AFM, at the lattice constant length scale, the AFM harbors a spin or magnetization profile that rapidly varies in space changing its sign from one lattice site to the next, which should manifest itself in physical observables. As a result, the AFM with its two sublattice magnetizations antiparallel to each other generates zero-spin Néel triplets [49]. Proceeding further along this line of thought, a homogeneous canted AFM with its sublattice magnetizations deviating from an antiparallel alignment effectively harbors a noncollinear spin texture capable of generating spinful triplet Cooper pairs in an adjacent S. This exciting possibility is theoretically examined in the present paper. Furthermore, a recent experiment [53] demonstrated generation and use of spinful triplet correlations employing the intrinsically noncollinear ground state of a kagome AFM.

Here, employing the Bogoliubov–de Gennes (BdG) framework [54], we theoretically investigate a bilayer structure consisting of an insulating AFM exchange coupled via a compensated interface to an adjacent S. We examine the critical temperature and spin-triplet correlations in the S as a function of the canting in the AFM, which allows us to continuously

*simran.chourasia@uam.es

tune the AFM from its collinear antiparallel state to it effectively becoming a FM. We find that Néel triplets are generated in the S both from the interband pairing channel considered recently [49] and from the conventional intraband pairing. The former channel is dominant at half filling, in which case states from two different electronic bands are energetically close to the chemical potential and can participate in forming these unconventional Néel triplet Cooper pairs [49]. This can be compared with pairing at finite energies in other multisublattice systems [55]. The conventional intraband pairing channel dominates away from half filling when only states within the same electronic band are energetically close to each other and the chemical potential. We find that the intraband pairing channel results in Néel triplet formation due to an imprinting of the Néel character by the AFM on the normal state electronic wave functions in the S. Although this channel of Néel triplet generation is found to be much weaker than the interband pairing channel, it admits qualitatively unique effects. We show that it is only in the intraband pairing channel that spinful Néel triplets are generated due to the intrinsic noncollinearity of a canted AFM. The S critical temperature variation as a function of the AFM canting angle is found to be consistent with the intraband Néel triplets being weaker than their interband counterparts, and may offer a convenient experimental signature of this interplay.

The paper is organized as follows. Section II introduces the model and BdG framework employed in our analysis. The dependence of spin-triplet correlations on space and AFM canting is discussed in Sec. III, while the variation of superconducting critical temperature is discussed in Sec. IV. Until this point, we consider a one-dimensional model that allows a simple and semianalytic understanding of the essential physics. In Sec. V, we employ a two-dimensional (2D) model for the S to validate our prior results and further examine the spatial dependence of the s-wave and p-wave triplet correlations. We conclude with discussion and summary of the key points in Sec. VI. The Appendixes provide details of the BdG framework, analytic evaluation of the normal state electronic properties in the bilayer, a discussion of the decay length of the spin-triplet correlations inside the S, critical temperature results for the 2D system, triplet correlations for a different configuration of the AFM sublattice magnetizations, and the parameters employed in our numerical routines.

II. AFM/S BILAYER MODEL

We consider a bilayer structure comprising an insulating AFM exchange coupled via a compensated interface to the S layer, as depicted schematically in Fig. 1(a). We anticipate that all three kinds of spin-triplet correlations will be generated in the S when the AFM sublattice magnetizations are canted [Fig. 1(a)]. We employ the Bogoliubov–de Gennes method and numerically evaluate the superconducting properties self-consistently [54]. The canted-AFM is taken to be an ideal insulator with a large band gap. Consequently, the Hamiltonian is formulated only for the itinerant electrons in S, as they never enter the insulating AFM. The AFM's influence on the S is accounted for by incorporating a spatially dependent spin splitting caused by the AFM spins [47,56,57]. Furthermore, with the aim of allowing a semianalytic understanding to the

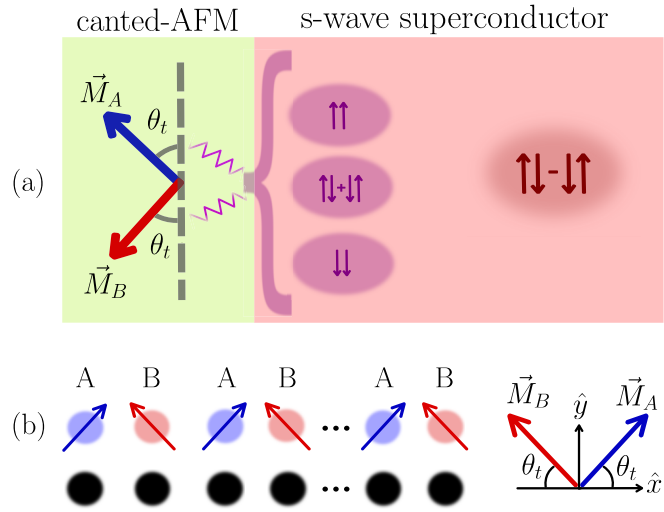

FIG. 1. (a) Schematic depiction of the system and key physics under investigation. Equal-spin and zero-spin triplet correlations are generated in a conventional s-wave spin-singlet superconductor when it is interfaced with a canted antiferromagnet (canted AFM). This results from the intrinsic noncollinearity between the two AFM sublattice magnetizations. (b) Schematic depiction of our model investigated using the Bogoliubov–de Gennes method. The black circles represent lattice sites of the superconductor hosting itinerant electrons and Cooper pairs. Blue (red) circles represent A (B) sublattice sites of the electrically insulating canted-AFM. The blue and red arrows denote the local AFM magnetic moments. The canting angle θ_t allows us to vary the magnet from being a collinear AFM ($\theta_t = 0$) to a ferromagnet ($\theta_t = \pi/2$).

essential physics, we consider a one-dimensional model as depicted schematically in Fig. 1(b). The resulting Hamiltonian is given by

$$H = -\mu \sum_{j,\sigma} c^{\dagger}_{j,\sigma} c_{j,\sigma} - t \sum_{\langle i,j \rangle} \sum_{\sigma} c^{\dagger}_{i,\sigma} c_{j,\sigma} - \frac{J}{2} \sum_{j} \vec{M}_j \cdot \vec{S}_j + \sum_{j} \left(\frac{|\Delta_j|^2}{U} + \Delta^*_j c_{j,\downarrow} c_{j,\uparrow} + \Delta_j c^{\dagger}_{j,\uparrow} c^{\dagger}_{j,\downarrow} \right), \quad (1)$$

where $c^{\dagger}_{j,\sigma}$ ($c_{j,\sigma}$) is the creation (annihilation) operator of an electron with spin σ at site j of the S layer, with $j = 1, 2, \ldots, N$ as the site index. Here, the spin quantization axis is taken along the z axis. We further consider periodic boundary conditions by allowing electrons to hop between sites $j = 1$ and $j = N$.

In Eq. (1), μ is the chemical potential. Within our theoretical method, it is determined via the filling factor f, which is the fraction of filled electronic states in the system. For $f = 0.5$ (half-filled band), we obtain $\mu = 0$. This corresponds to the Fermi wave-vector $k_F = \pi/2a$ located at the AFM Brillouin zone boundary (BZB), where a is the lattice constant. The normal state electronic dispersion and properties for the case of an AFM in its collinear antiparallel state have been discussed in Appendix A. For $f \neq 0.5$, μ is nonzero and the Fermi level is away from the AFM BZB. In the following analysis, we will consider the two qualitatively distinct cases of $f = 0.5$ and $f \neq 0.5$, corresponding to $\mu = 0$ and $\mu \neq 0$.

The second term in Eq. (1) is the kinetic energy term, describing hopping between nearest-neighboring sites $\langle i, j\rangle$ with $t > 0$ as the hopping parameter.

The third term in the Hamiltonian [Eq. (1)] accounts for the spin splitting due to the localized magnetic moments in the canted-AFM [6,47,58,59]. $J\vec{M}_j/2$ is the local spin-splitting field which causes an energy shift of spin-up and spin-down electrons by $\mp J/2$, with respect to the local spin-quantization axis along $\vec{M}_j$. The strength of this spin splitting, and thus the value of J in our model, depends on the S thickness and several other parameters [47]. It can thus be tuned in a broad range via appropriate thin film fabrication [47] as per the experimental requirements. Here, $\vec{M}_j = [(-1)^{j+1}\cos\theta_t\,\hat{x} + \sin\theta_t\,\hat{y}]$ is the unit vector along the direction of local magnetic moment at the jth canted-AFM site. The AFM sublattice magnetizations are taken to be in the x-y plane to examine the spin-triplet correlation with the quantization axis (z) perpendicular to this plane. A different magnetic configuration has also been investigated and discussed in the Appendixes. $\vec{S}_j = [(c^\dagger_{j,\uparrow}c_{j,\uparrow} - c^\dagger_{j,\downarrow}c_{j,\downarrow})\hat{z} + (c^\dagger_{j,\uparrow}c_{j,\downarrow} + c^\dagger_{j,\downarrow}c_{j,\uparrow})\hat{x} + (-ic^\dagger_{j,\uparrow}c_{j,\downarrow} + ic^\dagger_{j,\downarrow}c_{j,\uparrow})\hat{y}]$ is the spin operator of an electron at site j of the S.

The last term in Eq. (1) accounts for the conventional s-wave spin-singlet superconducting correlations. It is obtained by mean-field approximation of the pairing interaction $-U\sum_j n_{j,\uparrow}n_{j,\downarrow}$, where $U > 0$ is the attractive pairing potential and $n_{j,\sigma} = c^\dagger_{j,\sigma}c_{j,\sigma}$ is the number operator [54]. $\Delta_j = -U\langle c_{j,\downarrow}c_{j,\uparrow}\rangle$ is the resulting superconducting order parameter.

The total Hamiltonian Eq. (1) is numerically diagonalized and the superconducting state is determined self-consistently as detailed in Appendix B. The exact parameters employed in our numerical routines have been specified in Appendix E.

III. TRIPLET CORRELATIONS

In this section, we quantify and investigate the different spin-triplet correlations in the S. Consider the anomalous Matsubara Green's function $F_{jj,\sigma\sigma'}(\tau) = -\langle T_\tau c_{j,\sigma}(\tau)c_{j,\sigma'}(0)\rangle$, where $\tau = i\tilde{t}$ is the imaginary time with $\tilde{t}$ as the time [60,61]. Further, T_τ is the ordering operator for imaginary time τ. In the Fourier space, we obtain

$$F_{jj,\sigma\sigma'}(i\omega_l) = \int_0^\beta e^{i\omega_l\tau}F_{jj,\sigma\sigma'}(\tau)\,d\tau, \tag{2}$$

where $\beta = \hbar/k_BT$, k_B is the Boltzmann constant, T is the temperature, and $\omega_l = (2l+1)\pi/\beta$ are the fermionic Matsubara frequencies with integer l. See Appendix B for further calculation details. Since the spin-triplet correlations are odd in frequency [5], we take a sum over all positive Matsubara frequencies to define an appropriate dimensionless quantity that would allow us to quantify the correlations:

$$F_{j,\sigma\sigma'} = \frac{1}{\beta}\sum_{\omega_l>0}F_{jj,\sigma\sigma'}(i\omega_l). \tag{3}$$

Employing this notation, we express the relevant superconducting correlations

$$F^s_j = \frac{1}{2}(F_{j,\downarrow\uparrow} - F_{j,\uparrow\downarrow}), \tag{4}$$

$$F^{t,z}_j = -\frac{1}{2}(F_{j,\downarrow\uparrow} + F_{j,\uparrow\downarrow}), \tag{5}$$

$$F^{t,x}_j = \frac{1}{2}(F_{j,\uparrow\uparrow} - F_{j,\downarrow\downarrow}), \tag{6}$$

$$F^{t,y}_j = \frac{i}{2}(F_{j,\uparrow\uparrow} + F_{j,\downarrow\downarrow}). \tag{7}$$

F^s is the spin-singlet correlation. $F^{t,z}$, $F^{t,x}$, and $F^{t,y}$ are the zero-spin triplet correlations when spin is measured along the z, x, and y axes, respectively. Together, the latter three [Eqs. (5)–(7)] allow us to express all three kinds of the spin-triplet correlations with z quantization axis. We evaluate the quantities defined in Eqs. (4)–(7) to investigate the different superconducting correlations in our system.

A. Numerical results

In an isolated conventional S, only F^s is nonzero while $F^{t,x}$, $F^{t,y}$, and $F^{t,z}$ are zero. Now, if we consider a FM/S bilayer, then the propagating electronic wave functions in the normal state of the S film acquire a spin-dependent phase associated with their spin-dependent energies resulting from the spin-splitting induced by the FM [62]. The result is a relative phase difference between the opposite spin electrons as they propagate. In the superconducting state of the S layer, this causes the zero-spin triplet correlation with spin-quantization axis along the FM magnetization to become nonzero [5,62]. For example, if the magnetization of the FM is along the z axis, then $F^{t,z}$ becomes nonzero while $F^{t,x}$ and $F^{t,y}$ remain zero. Similarly, $F^{t,x}$ and $F^{t,y}$ become nonzero when magnetization of the ferromagnet is along the x and y axes, respectively.

Quasiclassical theory [60,61] shows that the triplet vector $\vec{F}^t_j = F^{t,x}_j\hat{x} + F^{t,y}_j\hat{y} + F^{t,z}_j\hat{z}$ always has a component aligning with the local exchange field $J\vec{M}_j/2$ whether the magnetization of the ferromagnet in a FM/S bilayer is homogeneous or inhomogeneous [4,63]. We, therefore, study these correlations to decompose the contribution of antiferromagnetic and ferromagnetic components of the canted-AFM.

For $\theta_t = 0$ (Fig. 1), our considered AFM becomes a collinear antiferromagnet with the axis of magnetic moments along the x direction. As we increase the value of θ_t by a small amount, the canted-AFM acquires a net magnetization along the y direction. So the canted-AFM can be decomposed into an AFM component (along the x axis) and a FM component (along the y axis). For a collinear AFM, we obtain Néel triplets. This means the component of $\vec{F}^t_j$ parallel to the axis of the Néel vector modulates with the Néel order of the AFM [49]. For $\theta_t = \pi/2$, we effectively obtain a FM/S structure with the FM magnetization along the y axis.

We now investigate the case of $\theta_t = \pi/4$ that produces maximum noncollinearity between the two AFM sublattice magnetization. In Fig. 2, triplet correlations for a canted-AFM/S bilayer have been plotted as a function of space for filling factor $f = 0.6$. We see that $F^{t,z}$, the component of $\vec{F}^t$ perpendicular to the canted-AFM sublattice magnetizations plane, is also being generated along with the in-plane components $F^{t,x}$ and $F^{t,y}$. It oscillates from a constant positive to negative value with Néel order. This oscillation can be

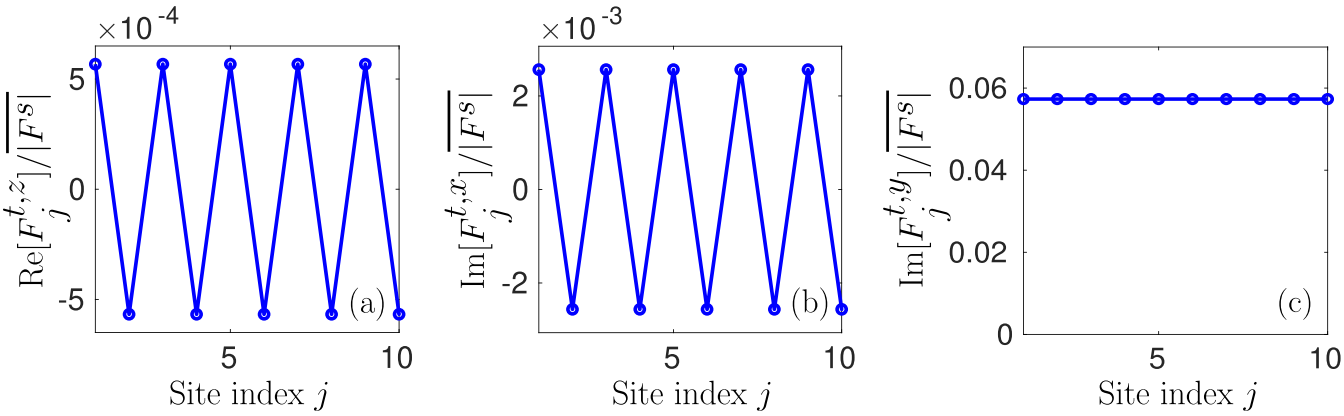

FIG. 2. Spatial variation of the normalized triplet correlations for ten lattice sites considering maximal noncollinearity corresponding to the canting angle $\theta_t = \pi/4$ and filling factor $f = 0.6$ ($\mu/\Delta_0 \approx 37$, where $2\Delta_0$ is the zero-temperature superconducting gap without the adjacent AFM). We plot the real part of the zero-spin triplet correlation $F_j^{t,z}$ (a), and the imaginary parts of the spin-triplet correlations $F_j^{t,x}$ (b), and $F_j^{t,y}$ (c). The imaginary part of the former and the real parts of the latter two are zero. All the correlations are normalized by the spatially averaged magnitude of the singlet correlation $\overline{|F^s|}$. The detailed parameters employed for the numerical evaluation are specified in Appendix E.

understood in terms of the noncollinearity that generates $F^{t,z}$. From one lattice site to the next, the angle between the spin splitting at the site and its direct neighbors is changing signs. However, $F^{t,z}$ only appears for nonzero μ and is zero at half filling ($f = 0.5$) where $\mu = 0$. $F^{t,x}$ too oscillates between a constant positive and negative value with Néel order, while $F^{t,y}$ is constant in space. Both $F^{t,x}$ and $F^{t,y}$ are imaginary, consistent with previous theoretical results for FM/S bilayers [62,63]. The AFM sublattice magnetization configuration has been chosen here to obtain and focus on the nonzero and spatially constant sum of the equal-spin triplets $F_{\uparrow\uparrow}$ and $F_{\downarrow\downarrow}$. In Appendix F, we present the correlations for a configuration when the AFM Néel order is aligned with the z axis [49]. To conclude this discussion, the intrinsic noncollinearity of the canted AFM successfully generates all three components of the spin-triplet correlations. The generation of spinful triplet Cooper pairs has conventionally been accomplished via the noncollinearity between the magnetizations of different FM layers [33].

We now examine the dependence of these spin triplets on the canting angle. To this end, we plot the average magnitudes of the three spin-triplet correlations versus the canting angle θ_t in Fig. 3. As we change θ_t from 0 to $\pi/2$, the system changes from a collinear AFM (along x axis) to a collinear F (along y axis). As discussed above, $F^{t,z}$ is found to vanish identically at $\mu = 0$ ($f = 0.5$) for all canting angles. This will be explained further below. However, for nonzero μ (away from the half-filling case), it increases from 0 to a finite value as we go from a collinear AFM alignment to maximal noncollinearity between the sublattice magnetic moments, and decreases back to zero in the ferromagnetic alignment [Fig. 3(a)]. This component thus results directly due to the AFM sublattice magnetization noncollinearity.

The spatially averaged value of $|F^{t,x}|$ decreases as θ_t goes from 0 to $\pi/2$ [Fig. 3(b)]. This component, therefore, essentially follows the Néel vector magnitude and appears to stem directly from the antiferromagnetism [49]. It has been understood as being due to the interband pairing, which is feasible when μ is smaller or comparable to the superconducting gap. However, we also find such Néel triplets to be present for $\mu \approx 37\Delta_0$ ($f = 0.6$), although they are significantly weaker than for the case of $\mu = 0$ [Fig. 3(b)]. We attribute this observation to a modification of the normal state electronic wave functions by the AFM, so even the conventional intraband pairing causes a finite generation of the Néel triplets. Finally, the average value of $|F^{t,y}|$ increases with the canting angle and appears to be caused primarily by the net magnetization.

B. Insights from simplified analytics

To understand the difference between $\mu = 0$ and $\mu \neq 0$ cases, we examine the electronic properties of a bilayer comprising a normal metal and an AFM, as detailed in Appendix A. For $\mu = 0$, the Fermi wave vector is $k_F = \pi/2a$. This means that the electrons participating in the formation of Cooper pairs have $|k| \sim \pi/2a$. The eigenfunctions with $|k| \sim \pi/2a$ are such that the probability of finding an electron is nonzero on one sublattice while it is zero on the other sublattice. Now, the electrons near the Fermi level of the S which interact with sublattice A do not see sublattice B and vice versa. Therefore, the triplet correlations are generated independently by sublattices A and B. The resultant correlations we obtain are a sum of correlations generated by the two sublattices. So, the only nonzero components are $F^{t,x}$ and $F^{t,y}$. This separation of the two sublattices at a special value of the electronic chemical potential is reminiscent of a similar result obtained for spin pumping via AFMs [64–67].

In contrast, for $\mu \neq 0$, the Fermi level is within one of the bands and the wave functions of the states near the Fermi energy are such that the electrons on a site of the A sublattice also have a nonzero probability at the sites of the B sublattice. There is no way for the electrons to arrange themselves to decouple the two sublattices [66,67]. The electrons experience a spin-splitting field in one direction at site 1 (of sublattice A) and in another direction at site 2 (of sublattice B), then again the first orientation at site 3 (of sublattice A). So, the electrons see the noncollinearity between the magnetic moments on the adjacent lattice sites. Therefore, the correlation $F^{t,z}$ along the direction perpendicular to the plane of magnetic moments of the canted-AFM becomes nonzero along with the in-plane components $F^{t,x}$ and $F^{t,y}$ when $\mu \neq 0$. At the same time,

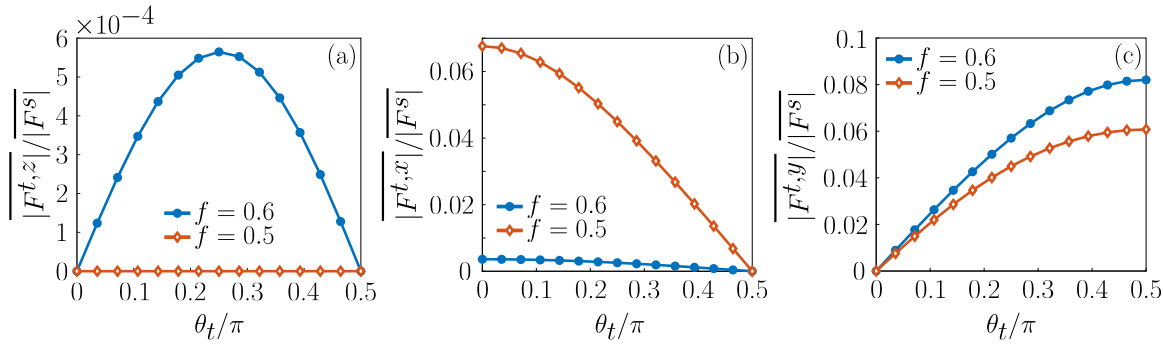

FIG. 3. Variation of triplet correlations with canting angle θ_t for filling factors $f = 0.5$ ($\mu = 0$) and $f = 0.6$ ($\mu/\Delta_0 \approx 37$), where Δ_0 represents the zero-temperature value of the superconducting order parameter in absence of the canted-AFM layer. (a) The average magnitude of the normalized spin-triplet correlation $F^{t,z}$ is maximum when the noncollinearity between the two sublattices is maximum, i.e., at $\theta_t = \pi/4$. However, it is zero at half filling ($f = 0.5$). (b) Average magnitude of the normalized spin-triplet correlation $F^{t,x} = [F_{\uparrow\uparrow} - F_{\downarrow\downarrow}]/2$ decreases as the effective antiferromagnetism becomes weaker with increasing θ_t. (c) The average magnitude of the normalized spin-triplet correlation $F^{t,y} = [i(F_{\uparrow\uparrow} + F_{\downarrow\downarrow})]/2$ increases as the effective ferromagnetism becomes stronger with increasing θ_t. The averages are taken over all sites and are denoted via an overhead bar. The detailed parameters employed for the numerical evaluation are specified in Appendix E.

the electronic amplitudes at the two sublattices are different due to the adjacent AFM, as detailed in Appendix A. This lends the normal electronic states a weak Néel character which manifests itself in the emergence of Néel triplets even for the conventional intraband pairing.

IV. CRITICAL TEMPERATURE

The formation of spin-triplet Cooper pairs comes at the cost of destroying their spin-singlet counterparts that are originally produced in and stabilize the superconducting state [59,68,69]. Hence, the critical temperature is reduced with the formation of spin-triplets, which may offer a convenient experimental signature. Thus, we investigate the critical temperature of our AFM/S bilayer now via numerical self-consistent solution of the BdG Eq. (1).

Critical temperature T_c versus canting angle θ_t is plotted in Fig. 4 for (a) $f = 0.5$ ($\mu = 0$) and (b) $f = 0.6$ ($\mu \approx 37\Delta_0$). We find that for $\mu = 0$, T_c increases with θ_t while it manifests the opposite dependence for $\mu \neq 0$. These intriguing and distinct dependencies can be understood based on our analysis of spin-triplets generation above.

Let us first consider the $f = 0.5$, corresponding to the $\mu = 0$ case presented in Fig. 4(a). In this case, a strong generation of spin-zero Néel triplets [Fig. 3(b)] due to interband pairing leads to maximal T_c suppression at $\theta_t = 0$. Hence, the T_c increases with θ_t since the T_c suppression is stronger for the collinear AFM case ($\theta_t = 0$) than for the FM case ($\theta_t = \pi/2$). Further, when the exchange field is large enough, we find a complete suppression of superconductivity at $\theta_t = 0$ corresponding to a vanishing T_c. The abrupt change in T_c with θ_t here is attributed to the additional contribution to superconductivity suppression by the opening of a normal dispersion band gap by the AFM, as described in Appendix A. This normal-state band gap predominantly affects the superconducting pairing at half filling when $\mu = 0$.

For the case of $f = 0.6$, the Néel spin triplet generation by the antiferromagnetic order is much weaker (Fig. 3). On the other hand, the ordinary spin-triplet generation by a FM remain of the same order of magnitude as for $f = 0.5$. Thus,

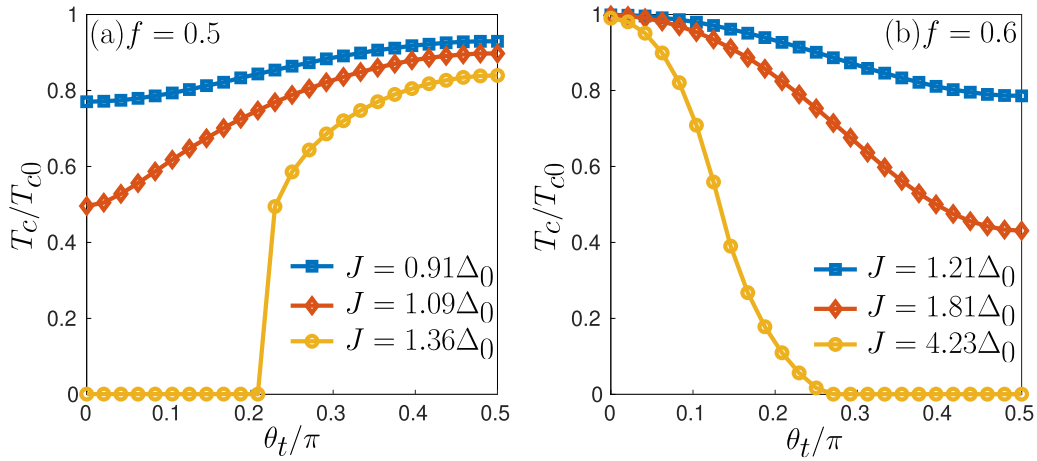

FIG. 4. (a) Normalized critical temperature T_c versus canting angle θ_t for filling factor (a) $f = 0.5$ and (b) $f = 0.6$ considering different values of the spin-splitting J. Here, T_{c0} and $2\Delta_0$ are, respectively, the critical temperature and the zero-temperature superconducting gap of the same superconductor without the AFM layer. The detailed parameters employed for the numerical evaluation are specified in Appendix E.

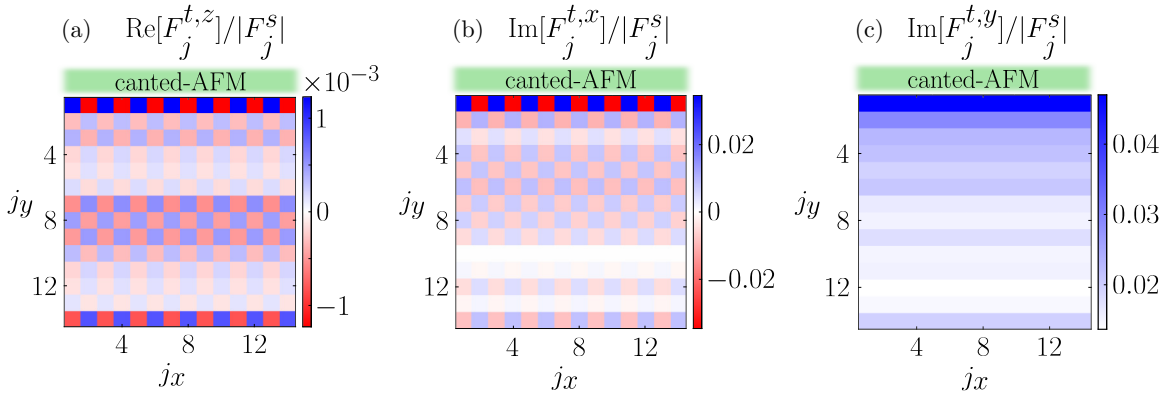

FIG. 5. Spatial variation of the spin-triplet correlations for a 2D superconductor. The sites are indexed as (j_x, j_y). The sites with index $(j_x, 1)$ form the layer adjacent to the AFM. A small section of size 14×14 of a superconducting sheet of size 102×14 has been plotted here for clarity. The real part of the normalized zero-spin triplet correlation $F_j^{t,z}$ (a), and the imaginary parts of the normalized spin-triplet correlations $F_j^{t,x}$ (b), and $F_j^{t,y}$ (c) have been plotted as color maps. The imaginary part of the former and real parts of the latter two are zero. We consider maximal noncollinearity ($\theta_t = \pi/4$) and filling fraction $f = 0.6$ ($\mu = 18.5\overline{|\Delta_0|}$). Here, $\overline{|\Delta_0|}$ is the average magnitude of the superconducting order parameter in absence of the canted-AFM layer and all the correlations are normalized with respect to the magnitude of the singlet correlation $|F_j^s|$. The detailed parameters employed for the numerical evaluation are specified in Appendix E.

T_c is largest for $\theta_t = 0$ and decreases with θ_t. The amplitude of spin triplets generated due to the noncollinearity [Fig. 3(a)] remains small and does not seem to affect the T_c dependence substantially. Contrary to the $\mu = 0$ case, the variation of T_c with θ_t is smooth even for large values of the exchange field J.

V. CORRELATIONS IN 2D

In our discussion above, we have considered a one-dimensional (1D) S with the aim of examining essential physics employing analytic results discussed in Appendix A. We now validate these results using a two-dimensional (2D) model for the S. This further allows us to examine how the spin-triplet correlations vary with space as we move away from the S/AFM interface.

In Fig. 1(b), the superconducting lattice is along the x axis. We add more such 1D layers in the y direction to create our 2D model for the S. Each site of this 2D sheet is indexed as (j_x, j_y) so j_x takes a value between 1 to N_x, and j_y takes a value between 1 to N_y, where N_x and N_y are the number of sites along x and y directions, respectively. The spin-splitting effect is experienced only by the electrons at the sites next to the AFM/S interface. Thus, it suffices to treat the AFM via the same 1D model as before. Overall, the Hamiltonian of Eq. (1) is modified by letting all site indices j take the form (j_x, j_y). Summation in the spin-splitting term is now over the sites with indices of the form $(j_x, 1)$. We continue to consider periodic boundary condition along the x axis, like in the 1D case.

Carrying out the BdG diagonalization self-consistently and numerically, we evaluate the spatially resolved spin-triplet correlations [Eqs. (4)–(7)] for this system and plot them in Fig. 5. We have the same observations in the first layer (along the AFM/S interface) of the 2D sheet as the 1D case discussed in Sec. III. Additional calculations not presented here confirm that $F^{t,z}$ appears only when μ is nonzero. We observe that $F^{t,x}$ and $F^{t,z}$ show modulation between positive and negative values along the y axis apart from along the x axis. This is interesting because the system has nothing imposing Néel order along the y axis on the correlations. In addition, we find some layers in which the alternating pattern of positive and negative values is skipped. This is attributed to Friedel-like oscillations [49,54]. We found that these skipping of patterns only appears for nonzero μ while we get a perfect alternating pattern along the y axis for $\mu = 0$ case. Although these Néel triplet correlations flip signs at the length scale of a lattice constant, their magnitude decays at the coherence length scale (shown in Appendix C). The correlation component $F^{t,y}$ [Fig. 5(c)] is constant in each layer along the interface (along the x axis) but decays as we move away from the interface along the y direction. So, the 2D case is consistent with and corroborates our 1D results, resulting in a similar trend in T_c suppression (Appendix D). We find that the spatial pattern (oscillating with Néel order or being constant in space) imposed on superconducting correlations along the interfacial direction also manifests itself perpendicular to the AFM/S interface.

In the 2D case, where the AFM/S interface breaks translational symmetry along the y axis, even-frequency p_y-wave spin-triplet correlations are created, in addition to the odd-frequency s-wave ones [13,15]. These are quantified as [70]

$$P_j^{t,z} = \frac{1}{8}[\langle c_{j,\downarrow} c_{j+\hat{y},\uparrow}\rangle + \langle c_{j,\uparrow} c_{j+\hat{y},\downarrow}\rangle - \langle c_{j,\downarrow} c_{j-\hat{y},\uparrow}\rangle - \langle c_{j,\uparrow} c_{j-\hat{y},\downarrow}\rangle], \tag{8}$$

$$P_j^{t,x} = \frac{1}{8}[-\langle c_{j,\uparrow} c_{j+\hat{y},\uparrow}\rangle + \langle c_{j,\downarrow} c_{j+\hat{y},\downarrow}\rangle + \langle c_{j,\uparrow} c_{j-\hat{y},\uparrow}\rangle - \langle c_{j,\downarrow} c_{j-\hat{y},\downarrow}\rangle], \tag{9}$$

$$P_j^{t,y} = \frac{i}{8}[-\langle c_{j,\uparrow} c_{j+\hat{y},\uparrow}\rangle - \langle c_{j,\downarrow} c_{j+\hat{y},\downarrow}\rangle + \langle c_{j,\uparrow} c_{j-\hat{y},\uparrow}\rangle + \langle c_{j,\downarrow} c_{j-\hat{y},\downarrow}\rangle], \tag{10}$$

where the site index $j \pm \hat{y} \equiv (j_x, j_y \pm 1)$ are the nearest neighbors of site j along the y axis, and $P_j^{t,\alpha}$ represent the zero-spin p_y-wave triplet correlation when the spin is measured along the α axis ($\alpha = x, y, z$).

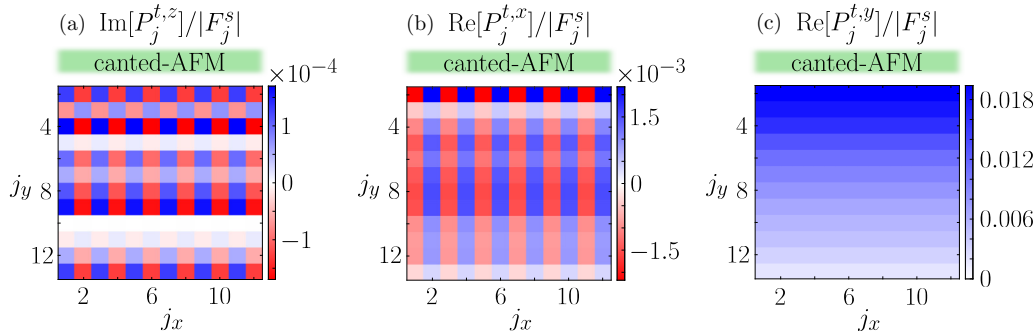

FIG. 6. Spatial variation of the p_y-wave triplet correlations in a 2D superconductor. The sites are indexed as (j_x, j_y). The sites with index $(j_x, 1)$ form the layer adjacent to the AFM. A small section of size 12×12 of a superconducting sheet of size 202×14 has been plotted here for clarity. The imaginary part of the normalized zero-spin p_y-wave triplet correlation $P_j^{t,z}$ (a) and the real parts of the normalized p_y-wave spin-triplet correlations $P_j^{t,x}$ (b) and $P_j^{t,y}$ (c) have been plotted here. The real part of the former and the imaginary parts of the latter two are zero. We consider maximal noncollinearity ($\theta_t = \pi/4$) and filling factor $f = 0.6$. All the correlations are normalized with respect to the magnitude of the s-wave singlet correlation $|F_j^s|$. The detailed parameters employed for the numerical evaluation are specified in Appendix E.

While the s-wave spin-triplets in Figs. 5(a)–5(b) nearly follow a checkerboard pattern, $P^{t,z}$ and $P^{t,x}$ tend to form stripes along the y direction [Figs. 6(a) and 6(b)] [71]. Unlike the on-site s-wave pairing, the p_y-wave pairing cannot take advantage of the complete decoupling of the two sublattices at half filling as they are defined on the link between sites in the A and B sublattices. For $P^{t,x}$, this can be seen by realizing that $\langle c_{j,\sigma} c_{j+\hat{y},\sigma}\rangle = -\langle c_{(j+\hat{y}),\sigma} c_{(j+\hat{y})-\hat{y},\sigma}\rangle$. Thus, if the link in the positive y direction from site j gives a positive contribution to $P^{t,x}$, then the link in the negative y direction from site $j+\hat{y}$ also gives a positive contribution, as can be seen by insertion into Eq. (9). Thus, a link from the A sublattice to the B sublattice and a link from the B sublattice to the A sublattice give a contribution to $P^{t,x}$ of the same sign. At half filling, the sign of $P^{t,x}$ is thus dictated by the sign of the spin splitting induced at the lattice site closest to the interface. Away from half filling, where the two sublattices are no longer perfectly decoupled, the perfect stripe pattern can be shifted along the x direction as can be seen for $P^{t,z}$ in Fig. 6(a). The ferromagnetic component $P_j^{t,y}$ in Fig. 6(c) remains positive inside the whole S, similar to the s-wave triplets in Fig. 5(c). Although we here observe qualitatively different behaviors in the nearest-neighbor (p-wave) pairing compared to the on-site (s-wave) one, we must note that the antiferromagnetic component and the component resulting from canting are both one order of magnitude larger for the latter. Thus, the AFM's influence on the critical temperature and other key superconducting properties is dominated by the odd-frequency s-wave Néel triplets generated in the S.

VI. CONCLUDING REMARKS

We have theoretically demonstrated the generation of all, including the spinful, spin-triplet Cooper pairs in a conventional S by an adjacent canted AFM. Our proposal leverages the intrinsic noncollinearity between the two sublattice magnetizations in a canted AFM for applications in superconducting hybrids. This canting can be induced intrinsically by Dzyaloshinskii-Moriya interaction, such as in hematite [72]. Additionally, it can be induced and controlled using an applied magnetic field [73]. The resulting spin triplets have a predominantly Néel character, i.e., their amplitude oscillates in space on the lattice length scale similar to the Néel spin order. While we have considered a lattice matched interface for concreteness and simplicity, the essential physics remains the same even in the presence of disorder with a gradual suppression of the Néel triplets with increasing disorder [49]. Furthermore, a metallic AFM would lead to similar phenomena as discussed here, with the additional complication of Cooper pairs leaking into the AFM. The superconducting critical temperature is more strongly suppressed by the interband Néel spin triplets than by a ferromagnetic spin-splitting field of similar magnitude, thereby offering an experimental signature of their generation. Altogether, our analysis highlights the noncollinear nature of homogeneous canted antiferromagnets by employing them for generating spin-triplet Cooper pairs in a simple superconducting bilayer. This manner of generating noncollinearity using a homogeneous AFM is expected to find use in other phenomena that have traditionally relied on magnetic multilayers or spin textures.

ACKNOWLEDGMENTS

S.C. and A.K. acknowledge financial support from the Spanish Ministry for Science and Innovation—AEI Grant No. CEX2018-000805-M (through the Maria de Maeztu Programme for Units of Excellence in R&D). L.J.K. acknowledges support from the Research Council of Norway through its Centres of Excellence funding scheme, Project No. 262633 QuSpin. I.V.B. acknowledges support from MIPT, Project No. FSMG-2023-0014.

APPENDIX A: NORMAL METAL INTERFACED WITH AN ANTIFERROMAGNET

To understand when interband and intraband pairing is favored, we consider the normal-state wave functions of an AFM/normal metal bilayer. The Hamiltonian for the conducting electrons of a normal metal interfaced with an insulating

AFM is modeled as [74]

$$H = -\mu \sum_{j,\sigma} c^{\dagger}_{j,\sigma} c_{j,\sigma} - t \sum_{\langle i,j \rangle} \sum_{\sigma} c^{\dagger}_{i,\sigma} c_{j,\sigma} - \frac{J}{2} \sum_{j} \vec{M}_j \cdot \vec{S}_j, \tag{A1}$$

where $\vec{M}_j = (-1)^{j+1}\hat{z}$ gives the magnetic texture of a collinear AFM. Other symbols have the same meaning as in Sec. II of the main text.

To calculate the eigenenergies and eigenvectors, the Hamiltonian is written in terms of creation and annihilation operators for electrons at sublattices A and B. Creation operators for electrons at sublattices A and B are defined as $a^{\dagger}_{j,\sigma} = c^{\dagger}_{2j-1,\sigma}$, and $b^{\dagger}_{j,\sigma} = c^{\dagger}_{2j,\sigma}$, where $j = 1, 2, \ldots, N/2$. Then, the basis is changed from Wannier wave functions to Bloch wave functions using the relations

$$\begin{aligned} a^{\dagger}_{j,\sigma} &= \sum_{k \in \mathrm{FBZ}} \frac{1}{\sqrt{N/2}} e^{-ik(2j-2)a} a^{\dagger}_{k,\sigma} \quad \text{and} \\ b^{\dagger}_{j,\sigma} &= \sum_{k \in \mathrm{FBZ}} \frac{1}{\sqrt{N/2}} e^{-ik(2j-1)a} b^{\dagger}_{k,\sigma}, \end{aligned} \tag{A2}$$

where a is the lattice constant and k is a reciprocal lattice vector in the FBZ. Now, the Hamiltonian can be written in the form

$$\begin{aligned} H = \sum_{k} & (a^{\dagger}_{k,\uparrow}\, a^{\dagger}_{k,\downarrow}\, b^{\dagger}_{k,\uparrow}\, b^{\dagger}_{k,\downarrow}) \\ & \times H(k) (a_{k,\uparrow}\, a_{k,\downarrow}\, b_{k,\uparrow}\, b_{k,\downarrow})^{T}, \end{aligned} \tag{A3}$$

giving the dispersion relation

$$E_{\pm}(k) = -\mu \pm \sqrt{4t^2 \cos^2(ka) + (J/2)^2}, \tag{A4}$$

where the two energy bands $E_{\pm}(k)$ are two-fold degenerate. The eigenvectors for energy band $E_{-}(k)$ are

$$\psi_1(k) = \mathcal{N}_2 \begin{pmatrix} 2t\cos(ka) \\ 0 \\ -J/2 + \sqrt{4t^2\cos^2(ka) + (J/2)^2} \\ 0 \end{pmatrix} = \begin{pmatrix} u^{(1)}_{Ak\uparrow} \\ u^{(1)}_{Ak\downarrow} \\ u^{(1)}_{Bk\uparrow} \\ u^{(1)}_{Bk\downarrow} \end{pmatrix} \tag{A5}$$

and

$$\psi_2(k) = \mathcal{N}_1 \begin{pmatrix} 0 \\ 2t\cos(ka) \\ 0 \\ J/2 + \sqrt{4t^2\cos^2(ka) + (J/2)^2} \end{pmatrix} = \begin{pmatrix} u^{(2)}_{Ak\uparrow} \\ u^{(2)}_{Ak\downarrow} \\ u^{(2)}_{Bk\uparrow} \\ u^{(2)}_{Bk\downarrow} \end{pmatrix}, \tag{A6}$$

whereas the eigenvectors for the energy band $E_{+}(k)$ are

$$\psi_3(k) = \mathcal{N}_1 \begin{pmatrix} 2t\cos(ka) \\ 0 \\ -J/2 - \sqrt{4t^2\cos^2(ka) + (J/2)^2} \\ 0 \end{pmatrix} = \begin{pmatrix} u^{(3)}_{Ak\uparrow} \\ u^{(3)}_{Ak\downarrow} \\ u^{(3)}_{Bk\uparrow} \\ u^{(3)}_{Bk\downarrow} \end{pmatrix} \tag{A7}$$

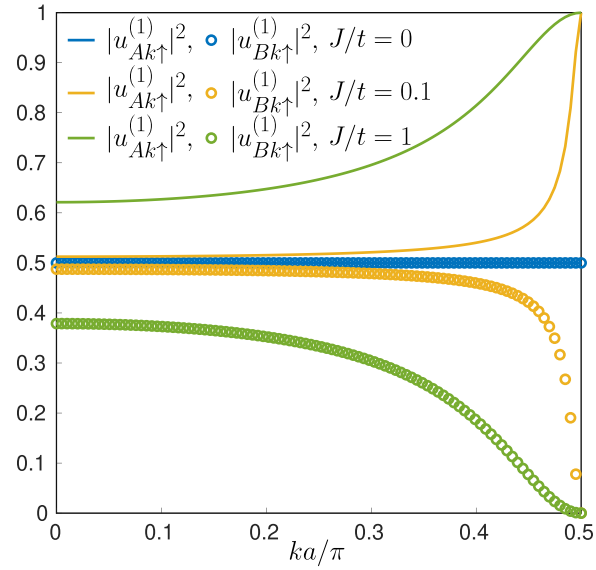

FIG. 7. Nonzero components of eigenfunction ψ_1 [Eq. (A5)] of a normal metal/AFM bilayer for different strengths of magnetic exchange interaction as a function of positive k values in the first Brillouin zone.

and

$$\psi_4(k) = \mathcal{N}_2 \begin{pmatrix} 0 \\ 2t\cos(ka) \\ 0 \\ J/2 - \sqrt{4t^2\cos^2(ka) + (J/2)^2} \end{pmatrix} = \begin{pmatrix} u^{(4)}_{Ak\uparrow} \\ u^{(4)}_{Ak\downarrow} \\ u^{(4)}_{Bk\uparrow} \\ u^{(4)}_{Bk\downarrow} \end{pmatrix}. \tag{A8}$$

Here, $\mathcal{N}_1$ and $\mathcal{N}_2$ are the normalization factors of the eigenvectors. ψ_1 and ψ_3 correspond to the wave functions of spin $\uparrow$ electrons, whereas ψ_2 and ψ_4 correspond to spin $\downarrow$ electrons. Figure 7 shows a plot of the nonzero components of ψ_1 for positive k values. Let us compare the case of $J = 0$ and $J \neq 0$ to study how the states of a metal are modified when it is brought in contact with an AFM.

From Fig. 7, we see that the probabilities of finding a spin $\uparrow$ electron at sites of sublattice A and B are equal for $J = 0$. However, for $J \neq 0$, the probability on the A sublattice is more than that on the B sublattice. It is important to note that the probability of finding spin $\uparrow$ electrons at sublattice A sites becomes 1 and that for sublattice B becomes 0 at $k = \pi/2a$. Similar asymmetries in the sublattices arise for states ψ_2, ψ_3, and ψ_4 as soon as we make J nonzero. For ψ_2, the probability of finding a spin $\downarrow$ electron at sublattice site B becomes more than that for sublattice A. For the states of $E_{+}(k)$ band (ψ_3 and ψ_4), the roles of sublattices A and B are interchanged with respect to spin.

Near the BZB of band $E_{-}(k)$ (i.e., ψ_1 and ψ_2), all the spin $\uparrow$ electrons get localized to the sites of sublattice A and all the spin $\downarrow$ electrons get localized to the sites of sublattice B. For the band $E_{+}(k)$, sublattices A and B interchange their roles and we find that spin $\uparrow$ electrons get localized at sublattice B and spin $\downarrow$ electrons get localized at sublattice A near the BZB. This property of the electronic states near the BZB is

the reason why interband pairing is the dominant mechanism for the formation of on-site opposite-spin Cooper pairs in an AFM/S bilayer when the Fermi level lies within the antiferromagnetic band gap $E_+ - E_-$. On the other hand, intraband pairing is the dominant mechanism when the Fermi level lies within one of the two bands.

APPENDIX B: BOGOLIUBOV-DE GENNES CALCULATION

The Hamiltonian in Eq. (1) can be written as

$$H = -\mu N + \sum_j \frac{|\Delta_j|^2}{U} + \frac{1}{2}\sum_{i,j} \Psi_i^\dagger \tilde{H}_{i,j} \Psi_j, \tag{B1}$$

where $\Psi_j^\dagger = (c_{j,\uparrow}^\dagger\, c_{j,\downarrow}^\dagger\, c_{j,\uparrow}\, c_{j,\downarrow})$ and N is the total number of sites. The matrix $\tilde{H}$ is diagonalized by solving the BdG equations

$$\sum_j \tilde{H}_{i,j}\phi_{j,n} = E_n \phi_{i,n}, \text{ where} \tag{B2}$$

$$\phi_{i,n} = (u_{i,n,\uparrow}\, u_{i,n,\downarrow}\, v_{i,n,\uparrow}\, v_{i,n,\downarrow})^T, \tag{B3}$$

is the eigenvector and E_n the eigenenergies of $\tilde{H}$. Now the Hamiltonian can be written as

$$H = -\mu N + \sum_j \frac{|\Delta_j|^2}{U} - \frac{1}{2}\tilde{\sum_n} E_n + \tilde{\sum_n} \Gamma_n^\dagger E_n \Gamma_n, \tag{B4}$$

where $\tilde{\sum}_n$ represents sum over positive eigenenergies and Γ_n's are Bogoliubov fermionic operators related to the old fermionic operators by $c_{j,\sigma} = \tilde{\sum}_n (u_{j,n,\sigma}\Gamma_n + v_{j,n,\sigma}^* \Gamma_n^\dagger)$. The superconducting order parameter is calculated self-consistently using the relation

$$\Delta_j = -U \tilde{\sum_n} [u_{j,n,\downarrow} v_{j,n,\uparrow}^* [1 - f_{\rm FD}(E_n)] + v_{j,n,\downarrow}^* u_{j,n,\uparrow} f_{\rm FD}(E_n)], \tag{B5}$$

where $f_{\rm FD}(E_n) = \langle \Gamma_n^\dagger \Gamma_n \rangle = 1/(e^{E_n/k_BT} + 1)$ is the Fermi-Dirac distribution.

To calculate the spin-triplet correlations, we consider the anomalous Matsubara Green's function $F_{jj,\sigma\sigma'}(\tau) = -\langle T_\tau c_{j,\sigma}(\tau) c_{j,\sigma'}(0)\rangle$, where $\tau = i\tilde{t}$ is the imaginary time, $\tilde{t}$ is the time, and T_τ is the ordering operator for τ. Taking its Fourier transform, we get

$$F_{jj,\sigma\sigma'}(i\omega_l) = \int_0^\beta e^{i\omega_l \tau} F_{jj,\sigma\sigma'}(\tau)\, d\tau = \tilde{\sum_n} \left[\frac{u_{j,n,\sigma} v_{j,n,\sigma'}^*}{i\omega_l - E_n/\hbar} + \frac{v_{j,n,\sigma}^* u_{j,n,\sigma'}}{i\omega_l + E_n/\hbar} \right], \tag{B6}$$

where $\beta = \hbar/k_BT$, k_B is the Boltzmann constant, T is the temperature, and $\omega_l = (2l+1)\pi/\beta$ is a Matsubara frequency for fermions with integer l. This expression is used in calculating the correlations in Eq. (3) and their relevant components Eqs. (4)–(7).

APPENDIX C: DECAY OF TRIPLET CORRELATIONS WITH DISTANCE IN 2-D

In Sec. V, we discussed the spatial variation of triplet correlations in a 2D S interfaced with a canted-AFM and observed that the Néel triplet correlations flip sign on adjacent sites to form a checkerboard pattern. In Fig. 8, we study the decay of the s-wave spin-triplet correlations with the distance from the AFM/S interface. We consider half filling ($f = 0.5$) to avoid the influence of Friedel oscillations. We observe that the magnitude of both the ferromagnetic and antiferromagnetic

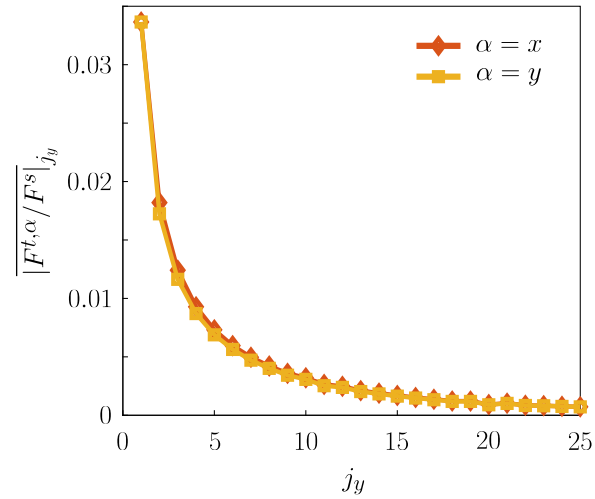

FIG. 8. The average magnitude of the s-wave spin-triplet correlations normalized by the singlet correlation in each j_y layer parallel to the canted-AFM/S interface ($\overline{|F^{t,\alpha}/F^s|}_{j_y}$, $\alpha = x, y$) is plotted with respect to the distance from the interface. We consider half filling ($f = 0.5$) and maximal canting ($\theta_t = \pi/4$). The sites with index $j_y = 1$ form the layer adjacent to the AFM. Ignoring the edge effects, we show only the first 25 layers of a superconducting sheet with 102×30 sites. The $F^{t,z}$ component is zero in all the layers. The detailed parameters employed for the numerical evaluation are specified in Appendix E.

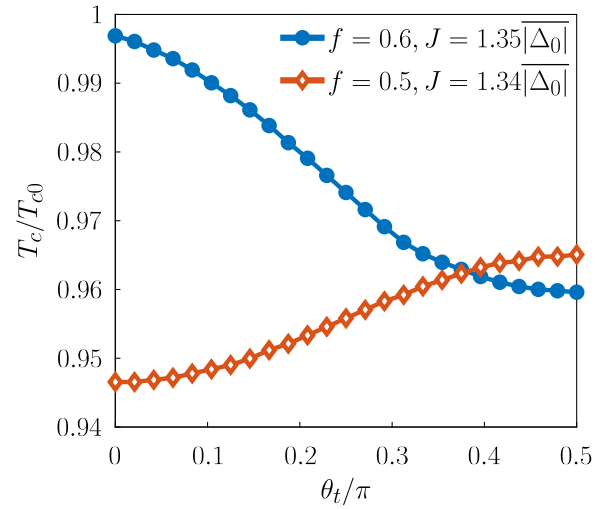

FIG. 9. The critical temperature T_c versus canting angle θ_t is plotted for a 2D superconductor of size 302×3 interfaced with a canted-AFM at filling factors $f = 0.5$ and $f = 0.6$. T_{c0} and $\overline{|\Delta_0|}$ are the critical temperature and the average superconducting order parameter at zero-temperature, respectively, in the absence of the magnetic layer. The detailed parameters employed for the numerical evaluation are specified in Appendix E.

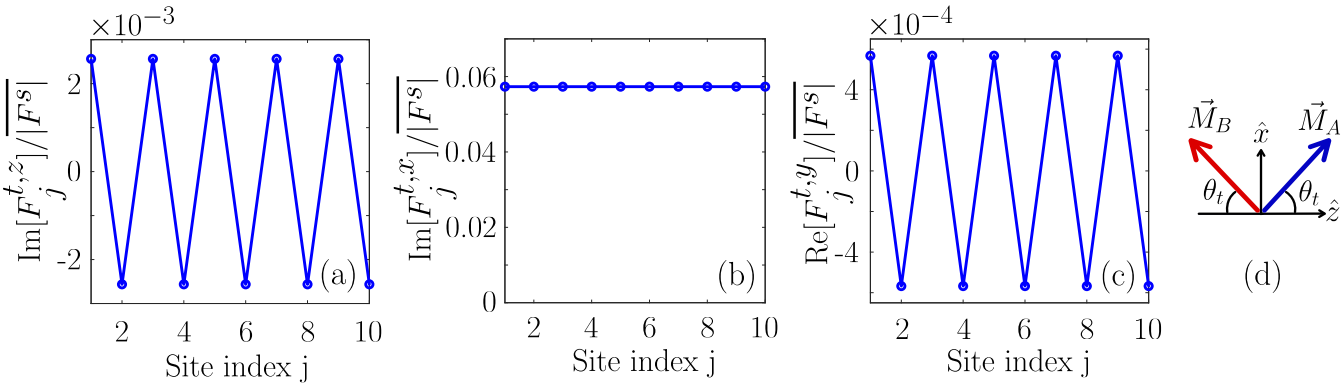

FIG. 10. Spatial variation of normalized triplet correlations for ten lattice sites considering $\theta_t = \pi/4$ and $\mu/\Delta_0 = 37$, corresponding to filling factor $f = 0.6$. We show the imaginary part of the triplet correlations $F_j^{t,z}$ (a) and $F_j^{t,x}$ (b), and the real part of the triplet correlation $F_j^{t,y}$ (c). The real part of the two former and the imaginary parts of the latter are zero. All correlations are normalized by the spatially averaged magnitude of the singlet correlation $\overline{|F^s|}$. (d) Orientation of the magnetic moments of sublattices A and B of the AFM in the rotated configuration.

components of the correlations decay exponentially over a length scale determined by the coherence length. The rapid oscillations of the Néel order of the canted-AFM over the atomic length scale thus only affects the sign of the triplet correlations.

APPENDIX D: CRITICAL TEMPERATURE OF 2-D S/CANTED-AFM

In Sec. IV, we found that the critical temperature versus canting angle curves of a 1D S show opposite trends at half filling ($f = 0.5$) and away from half filling ($f = 0.6$). In Fig. 9, we show that T_c behaves similarly for a 2D S. The change in T_c as we change the canting angle from the collinear AFM case ($\theta_t = 0$) to the FM case ($\theta_t = \pi/2$), however, decreases in magnitude. This is because, with an increasing S thickness, the effective spin-splitting induced by the AFM decreases.

APPENDIX E: NUMERICAL PARAMETERS

The parameters used for each of the figures are

(1) Figure 2: A 1D S with number of sites $N = 302$, hopping parameter $t = 10$, pair potential $U/t = 1$, magnetic exchange interaction strength $J = 0.018\,t$ ($= 1.09\Delta_0$), canting angle $\theta_t = \pi/4$, and filling factor $f = 0.6$ ($\mu/\Delta_0 = 37$), at temperature $T = 0.1\,T_c = 0.001\,t/k_B$ is taken to calculate s-wave triplet correlations. Here, $2\Delta_0$ is the zero-temperature superconducting gap without the adjacent AFM.

(2) Figure 3: A 1D S with $N = 302$, $t = 10$, and $U/t = 1$ at $k_BT/t = 0.001$ is taken for calculating correlations. For filling factor $f = 0.5$ ($\mu/\Delta_0 = 0$), $J = 0.012\,t = 1.09\Delta_0$ is taken, and for $f = 0.6$ ($\mu/\Delta_0 = 37$), $J = 0.018\,t = 1.09\Delta_0$, is taken. Here, $2\Delta_0$ represents the superconducting gap in the absence of the canted-AFM at zero-temperature.

(3) Figure 4: A 1D S with $N = 302$, $t = 10$, $U/t = 1$ is used for the calculation of T_c for filling factors $f = 0.5$ ($\mu/\Delta_0 = 0$) and $f = 0.6$ ($\mu/\Delta_0 = 37$). The critical temperature of the isolated S T_{c0} for $f = 0.6$ is $0.0101\,t/k_B$ and for $f = 0.5$ is $0.0076\,t/k_B$.

(4) Figure 5: A 2D superconducting sheet with $N_x = 102$, $N_y = 14$, $t = 10$, $J = 0.1\,t = 4.3\,\overline{|\Delta_0|}$, $\theta_t = \pi/4$, $U/t = 1$, and $f = 0.6$ ($\mu/\overline{|\Delta_0|} = 18.5$) at $k_BT/t = 0.001$ is used to calculate the s-wave triplet correlations. Here, $\overline{|\Delta_0|}$ represents the average magnitude of the superconducting order parameter in absence of the canted-AFM layer.

(5) Figure 6: A 2-D S with $N_x = 202$, $N_y = 14$, $t = 10$, $J = 0.1\,t = 4.3\,\overline{|\Delta_0|}$, $\theta_t = \pi/4$, $U/t = 1$, and $f = 0.6$ ($\mu/\overline{|\Delta_0|} = 18$) at $k_BT/t = 0.001$ is used to calculate the p_y-wave triplet correlations. Here, $\overline{|\Delta_0|}$ represents the average magnitude of the superconducting order parameter in absence of the AFM.

(6) Figure 8: A 2D S with $N_x = 102$, $N_y = 30$, $t = 10$, $J = 0.1\,t = 1.7\,\overline{|\Delta_0|}$, $\theta_t = \pi/4$, $U/t = 1$, and $f = 0.5$ ($\mu = 0$) at $k_BT/t = 0.001$ is used to calculate the s-wave triplet correlations, where $\overline{|\Delta_0|}$ represents the average magnitude of the superconducting order parameter in absence of the AFM.

(7) Figure 9: A 2D S with $N_x = 302$, $N_y = 3$, $t = 10$, and $U/t = 1$ is used to plot T_c versus θ_t. For $f = 0.5$, $J = 0.047\,t = 1.34\,\overline{|\Delta_0|} = 2.4\,T_{c0}$ is taken, and for $f = 0.6$, $J = 0.07\,t = 1.35\,\overline{|\Delta_0|} = 2.4\,T_{c0}$ is taken, where T_{c0} and $\overline{|\Delta_0|}$ are the critical temperature and the average magnitude of the superconducting order parameter at zero temperature of the same S without the AFM layer.

APPENDIX F: CANTED-AFM/S WITH ROTATED MAGNETIC MOMENTS

To compare the results of this paper with Ref. [49], one needs to rotate the magnetic moments of the Hamiltonian [Eq. (1)] to $\vec{M}_j = [(-1)^{j+1}\cos\theta_t\,\hat{z} + \sin\theta_t\,\hat{x}]$ [see Fig. 10(d)]. The correlations for this rotated system is plotted in Fig. 10. Here, $F^{t,z}$ is the Néel triplet correlation coming from the antiferromagnetic component of the canted-AFM, $F^{t,x}$ comes from the ferromagnetic component, and $F^{t,y}$ comes from the noncollinearity in the canted AFM.

[1] Z.-L. Xiang, S. Ashhab, J. Q. You, and F. Nori, Hybrid quantum circuits: Superconducting circuits interacting with other quantum systems, Rev. Mod. Phys. **85**, 623 (2013).

[2] P. Krantz, M. Kjaergaard, F. Yan, T. P. Orlando, S. Gustavsson, and W. D. Oliver, A quantum engineer's guide to superconducting qubits, Appl. Phys. Rev. **6**, 021318 (2019).

[3] M. Sigrist and K. Ueda, Phenomenological theory of unconventional superconductivity, Rev. Mod. Phys. **63**, 239 (1991).

[4] M. Eschrig, Spin-polarized supercurrents for spintronics: A review of current progress, Rep. Prog. Phys. **78**, 104501 (2015).

[5] F. S. Bergeret, A. F. Volkov, and K. B. Efetov, Odd triplet superconductivity and related phenomena in superconductor-ferromagnet structures, Rev. Mod. Phys. **77**, 1321 (2005).

[6] F. S. Bergeret, M. Silaev, P. Virtanen, and T. T. Heikkilä, Colloquium: Nonequilibrium effects in superconductors with a spin-splitting field, Rev. Mod. Phys. **90**, 041001 (2018).

[7] A. I. Buzdin, Proximity effects in superconductor-ferromagnet heterostructures, Rev. Mod. Phys. **77**, 935 (2005).

[8] J. Linder and J. W. A. Robinson, Superconducting spintronics, Nat. Phys. **11**, 307 (2015).

[9] G. Yang, C. Ciccarelli, and J. W. A. Robinson, Boosting spintronics with superconductivity, APL Mater. **9**, 050703 (2021).

[10] I. V. Bobkova, A. M. Bobkov, and M. A. Silaev, Spin torques and magnetic texture dynamics driven by the supercurrent in superconductor/ferromagnet structures, Phys. Rev. B **98**, 014521 (2018).

[11] X. Waintal and P. W. Brouwer, Magnetic exchange interaction induced by a Josephson current, Phys. Rev. B **65**, 054407 (2002).

[12] K. Halterman and M. Alidoust, Josephson currents and spin-transfer torques in ballistic SFSFS nanojunctions, Supercond. Sci. Technol. **29**, 055007 (2016).

[13] J. Linder and T. Yokoyama, Supercurrent-induced magnetization dynamics in a Josephson junction with two misaligned ferromagnetic layers, Phys. Rev. B **83**, 012501 (2011).

[14] L. Fu and C. L. Kane, Superconducting Proximity Effect and Majorana Fermions at the Surface of a Topological Insulator, Phys. Rev. Lett. **100**, 096407 (2008).

[15] Y. Tanaka, M. Sato, and N. Nagaosa, Symmetry and topology in superconductors—odd-frequency pairing and edge states, J. Phys. Soc. Jpn. **81**, 011013 (2012).

[16] M. Eschrig and T. Löfwander, Triplet supercurrents in clean and disordered half-metallic ferromagnets, Nat. Phys. **4**, 138 (2008).

[17] R. S. Keizer, S. T. B. Goennenwein, T. M. Klapwijk, G. Miao, G. Xiao, and A. Gupta, A spin triplet supercurrent through the half-metallic ferromagnet CrO_2, Nature (London) **439**, 825 (2006).

[18] T. S. Khaire, M. A. Khasawneh, W. P. Pratt, and N. O. Birge, Observation of Spin-triplet Superconductivity in Co-based Josephson Junctions, Phys. Rev. Lett. **104**, 137002 (2010).

[19] K.-R. Jeon, C. Ciccarelli, A. J. Ferguson, H. Kurebayashi, L. F. Cohen, X. Montiel, M. Eschrig, J. W. A. Robinson, and M. G. Blamire, Enhanced spin pumping into superconductors provides evidence for superconducting pure spin currents, Nat. Mater. **17**, 499 (2018).

[20] K.-R. Jeon, X. Montiel, S. Komori, C. Ciccarelli, J. Haigh, H. Kurebayashi, L. F. Cohen, A. K. Chan, K. D. Stenning, C.-M. Lee, M. Eschrig, M. G. Blamire, and J. W. A. Robinson, Tunable Pure Spin Supercurrents and the Demonstration of Their Gateability in a Spin-wave Device, Phys. Rev. X **10**, 031020 (2020).

[21] S. Diesch, P. Machon, M. Wolz, C. Sürgers, D. Beckmann, W. Belzig, and E. Scheer, Creation of equal-spin triplet superconductivity at the Al/EuS interface, Nat. Commun. **9**, 5248 (2018).

[22] A. Costa, M. Sutula, V. Lauter, J. Song, J. Fabian, and J. S. Moodera, Signatures of superconducting triplet pairing in Ni-Ga-bilayer junctions, New J. Phys. **24**, 033046 (2022).

[23] A. Hijano, V. N. Golovach, and F. S. Bergeret, Quasiparticle density of states and triplet correlations in superconductor/ferromagnetic-insulator structures across a sharp domain wall, Phys. Rev. B **105**, 174507 (2022).

[24] J. W. A. Robinson, J. D. S. Witt, and M. G. Blamire, Controlled injection of spin-triplet supercurrents into a strong ferromagnet, Science **329**, 59 (2010).

[25] F. Chiodi, J. D. S. Witt, R. G. J. Smits, L. Qu, G. B. Halász, C.-T. Wu, O. T. Valls, K. Halterman, J. W. A. Robinson, and M. G. Blamire, Supra-oscillatory critical temperature dependence of Nb-Ho bilayers, Europhys. Lett. **101**, 37002 (2013).

[26] C. González-Ruano, L. G. Johnsen, D. Caso, C. Tiusan, M. Hehn, N. Banerjee, J. Linder, and F. G. Aliev, Superconductivity-induced change in magnetic anisotropy in epitaxial ferromagnet-superconductor hybrids with spin-orbit interaction, Phys. Rev. B **102**, 020405(R) (2020).

[27] C.-T. Wu, O. T. Valls, and K. Halterman, Reentrant Superconducting Phase in Conical-Ferromagnet–Superconductor Nanostructures, Phys. Rev. Lett. **108**, 117005 (2012).

[28] N. Banerjee, J. A. Ouassou, Y. Zhu, N. A. Stelmashenko, J. Linder, and M. G. Blamire, Controlling the superconducting transition by spin-orbit coupling, Phys. Rev. B **97**, 184521 (2018).

[29] L. G. Johnsen, N. Banerjee, and J. Linder, Magnetization reorientation due to the superconducting transition in heavy-metal heterostructures, Phys. Rev. B **99**, 134516 (2019).

[30] S. H. Jacobsen, J. A. Ouassou, and J. Linder, Critical temperature and tunneling spectroscopy of superconductor-ferromagnet hybrids with intrinsic Rashba-Dresselhaus spin-orbit coupling, Phys. Rev. B **92**, 024510 (2015).

[31] S. Tamura, Y. Tanaka, and T. Yokoyama, Generation of polarized spin-triplet cooper pairings by magnetic barriers in superconducting junctions, Phys. Rev. B **107**, 054501 (2023).

[32] P. Dutta and A. M. Black-Schaffer, Signature of odd-frequency equal-spin triplet pairing in the Josephson current on the surface of Weyl nodal loop semimetals, Phys. Rev. B **100**, 104511 (2019).

[33] P. V. Leksin, N. N. Garif'yanov, I. A. Garifullin, Y. V. Fominov, J. Schumann, Y. Krupskaya, V. Kataev, O. G. Schmidt, and B. Büchner, Evidence for Triplet Superconductivity in a Superconductor-Ferromagnet Spin Valve, Phys. Rev. Lett. **109**, 057005 (2012).

[34] A. I. Buzdin and M. Y. Kupriyanov, Transition-temperature of a superconductor-ferromagnet superlattice, Pis'ma Zh. Eksp. Teor. Fiz. **52**, 1089 (1990) [JETP Lett. **52**, 487 (1990)].

[35] Z. Radović, M. Ledvij, L. Dobrosavljević-Grujić, A. I. Buzdin, and J. R. Clem, Transition temperatures of superconductor-ferromagnet superlattices, Phys. Rev. B **44**, 759 (1991).

[36] J. J. Hauser, H. C. Theuerer, and N. R. Werthamer, Proximity effects between superconducting and magnetic films, Phys. Rev. **142**, 118 (1966).

[37] M. Hübener, D. Tikhonov, I. A. Garifullin, K. Westerholt, and H. Zabel, The antiferromagnet/superconductor proximity effect in Cr/V/Cr trilayers, J. Phys.: Condens. Matter **14**, 8687 (2002).

[38] C. Bell, E. J. Tarte, G. Burnell, C. W. Leung, D.-J. Kang, and M. G. Blamire, Proximity and Josephson effects in superconductor/antiferromagnetic $Nb/\gamma - Fe_{50}Mn_{50}$ heterostructures, Phys. Rev. B **68**, 144517 (2003).

[39] B. L. Wu, Y. M. Yang, Z. B. Guo, Y. H. Wu, and J. J. Qiu, Suppression of superconductivity in Nb by IrMn in IrMn/Nb bilayers, Appl. Phys. Lett. **103**, 152602 (2013).

[40] R. L. Seeger, G. Forestier, O. Gladii, M. Leiviskä, S. Auffret, I. Joumard, C. Gomez, M. Rubio-Roy, A. I. Buzdin, M. Houzet, and V. Baltz, Penetration depth of cooper pairs in the IrMn antiferromagnet, Phys. Rev. B **104**, 054413 (2021).

[41] A. Mani, T. G. Kumary, D. Hsu, J. G. Lin, and C.-H. Chern, Modulation of superconductivity by spin canting in a hybrid antiferromagnet/superconductor oxide, Appl. Phys. Lett. **94**, 072509 (2009).

[42] A. Mani, T. G. Kumary, and J. G. Lin, Thickness controlled proximity effects in c-type antiferromagnet/superconductor heterostructure, Sci. Rep. **5**, 12780 (2015).

[43] I. V. Bobkova, P. J. Hirschfeld, and Y. S. Barash, Spin-Dependent Quasiparticle Reflection and Bound States at Interfaces with Itinerant Antiferromagnets, Phys. Rev. Lett. **94**, 037005 (2005).

[44] B. M. Andersen, I. V. Bobkova, P. J. Hirschfeld, and Y. S. Barash, $0 - \pi$ Transitions in Josephson Junctions with Antiferromagnetic Interlayers, Phys. Rev. Lett. **96**, 117005 (2006).

[45] B. M. Andersen, I. V. Bobkova, P. J. Hirschfeld, and Y. S. Barash, Bound states at the interface between antiferromagnets and superconductors, Phys. Rev. B **72**, 184510 (2005).

[46] M. F. Jakobsen, K. B. Naess, P. Dutta, A. Brataas, and A. Qaiumzadeh, Electrical and thermal transport in antiferromagnet-superconductor junctions, Phys. Rev. B **102**, 140504(R) (2020).

[47] A. Kamra, A. Rezaei, and W. Belzig, Spin Splitting Induced in a Superconductor by an Antiferromagnetic Insulator, Phys. Rev. Lett. **121**, 247702 (2018).

[48] L. G. Johnsen, S. H. Jacobsen, and J. Linder, Magnetic control of superconducting heterostructures using compensated antiferromagnets, Phys. Rev. B **103**, L060505 (2021).

[49] G. A. Bobkov, I. V. Bobkova, A. M. Bobkov, and A. Kamra, Néel proximity effect at antiferromagnet/superconductor interfaces, Phys. Rev. B **106**, 144512 (2022).

[50] V. Baltz, A. Manchon, M. Tsoi, T. Moriyama, T. Ono, and Y. Tserkovnyak, Antiferromagnetic spintronics, Rev. Mod. Phys. **90**, 015005 (2018).

[51] E. H. Fyhn, A. Brataas, A. Qaiumzadeh, and J. Linder, Superconducting Proximity Effect and Long-Ranged Triplets in Dirty Metallic Antiferromagnets, Phys. Rev. Lett. **131**, 076001 (2023).

[52] S. I. Pekar and E. I. Rashba, Combined resonance in crystals in inhomogeneous magnetic fields, J. Exp. Theor. Phys. **20**, 1295 (1965).

[53] K.-R. Jeon, B. K. Hazra, J.-K. Kim, J.-C. Jeon, H. Han, H. L. Meyerheim, T. Kontos, A. Cottet, and S. S. P. Parkin, Chiral antiferromagnetic Josephson junctions as spin-triplet supercurrent spin valves and d.c. SQUIDs, Nat. Nanotechnol. **18**, 747 (2023).

[54] J. Zhu, *Bogoliubov-de Gennes Method and Its Applications*, Lecture Notes in Physics (Springer International Publishing, Switzerland, 2016).

[55] G. Tang, C. Bruder, and W. Belzig, Magnetic Field-Induced "Mirage" Gap in an Ising Superconductor, Phys. Rev. Lett. **126**, 237001 (2021).

[56] A. Cottet, D. Huertas-Hernando, W. Belzig, and Y. V. Nazarov, Spin-dependent boundary conditions for isotropic superconducting Green's functions, Phys. Rev. B **80**, 184511 (2009).

[57] M. Eschrig, A. Cottet, W. Belzig, and J. Linder, General boundary conditions for quasiclassical theory of superconductivity in the diffusive limit: Application to strongly spin-polarized systems, New J. Phys. **17**, 083037 (2015).

[58] M. Kiwi, Exchange bias theory, J. Magn. Magn. Mater. **234**, 584 (2001).

[59] K. Maki and T. Tsuneto, Pauli paramagnetism and superconducting state, Prog. Theor. Phys. **31**, 945 (1964).

[60] N. Kopnin, *Theory of Nonequilibrium Superconductivity*, International Series of Monographs (Clarendon Press, Oxford, 2001).

[61] W. Belzig, F. K. Wilhelm, C. Bruder, G. Schön, and A. D. Zaikin, Quasiclassical Green's function approach to mesoscopic superconductivity, Superlattices Microstruct. **25**, 1251 (1999).

[62] M. Eschrig, T. Löfwander, T. Champel, J. C. Cuevas, J. Kopu, and G. Schön, Symmetries of pairing correlations in superconductor-ferromagnet nanostructures, J. Low Temp. Phys. **147**, 457 (2007).

[63] T. Champel and M. Eschrig, Effect of an inhomogeneous exchange field on the proximity effect in disordered superconductor-ferromagnet hybrid structures, Phys. Rev. B **72**, 054523 (2005).

[64] S. Takei, B. I. Halperin, A. Yacoby, and Y. Tserkovnyak, Superfluid spin transport through antiferromagnetic insulators, Phys. Rev. B **90**, 094408 (2014).

[65] R. Cheng, J. Xiao, Q. Niu, and A. Brataas, Spin Pumping and Spin-Transfer Torques in Antiferromagnets, Phys. Rev. Lett. **113**, 057601 (2014).

[66] A. Kamra and W. Belzig, Spin Pumping and Shot Noise in Ferrimagnets: Bridging Ferro- and Antiferromagnets, Phys. Rev. Lett. **119**, 197201 (2017).

[67] Q. Liu, H. Y. Yuan, K. Xia, and Z. Yuan, Mode-dependent damping in metallic antiferromagnets due to intersublattice spin pumping, Phys. Rev. Mater. **1**, 061401(R) (2017).

[68] B. S. Chandrasekhar, A note on the maximum critical field of high-sfield superconductors, Appl. Phys. Lett. **1**, 7 (1962).

[69] A. M. Clogston, Upper Limit for the Critical Field in Hard Superconductors, Phys. Rev. Lett. **9**, 266 (1962).

[70] L. A. B. Olde Olthof, L. G. Johnsen, J. W. A. Robinson, and J. Linder, Controllable Enhancement of p-Wave Superconductivity Via Magnetic Coupling to a Conventional Superconductor, Phys. Rev. Lett. **127**, 267001 (2021).

[71] As the p_y-wave triplet correlations are not defined at the edges, we plot these starting at the second row of lattice sites from the edge.

[72] A. H. Morrish, *Canted Antiferromagnetism: Hematite* (World Scientific, Singapore, 1995).

[73] T. Wimmer, A. Kamra, J. Gückelhorn, M. Opel, S. Geprägs, R. Gross, H. Huebl, and M. Althammer, Observation of Antiferromagnetic Magnon Pseudospin Dynamics and the Hanle Effect, Phys. Rev. Lett. **125**, 247204 (2020).

[74] H. T. Simensen, A. Kamra, R. E. Troncoso, and A. Brataas, Magnon decay theory of gilbert damping in metallic antiferromagnets, Phys. Rev. B **101**, 020403(R) (2020).